University of Twente

EEMCS / Electrical Engineering
Robotics and *Mechatronics*

Design of control strategies for UAVs physically interacting with each other and the environment

R.T.L.M. (Ramon) Tummers

MSc Report

Committee:
Prof.dr.ir. S. Stramigioli
Dr. R. Carloni
Mr. M. Fumagalli, PhD
Dr.ir. R.G.K.M. Aarts

December 2012

Report nr. 032RAM2012
Robotics and Mechatronics
EE-Math-CS
University of Twente
P.O. Box 217
7500 AE Enschede
The Netherlands

Contents

General introduction

The field of autonomous aerial service robots increased significantly in the last couple of years. The main motivation behind this is the growing wish to be able to do tasks at hard to reach places, e.g. skyscrapers and windmills. Here labour costs can be reduced significanly when aerial vehicles are used in stead of regular personnel as they need expensive machinery and/or scaffolding to reach these places.

When these unmanned aerial vehicles (UAVs) will be used in real application scenarios like the ones mentioned above, the ability to interact actively and safely with the environment is required. Also interaction between several UAVs is of importance as some tasks might by impossible to conduct with only one UAV. All this interaction takes place in free-flight, so without constraints to the ground.

The main goal of the research presented in this report is to design a control architecture that complies with these requirements. This design will be done through simulation and experimental validation of a quadrotor UAV endowed with an edge mounted robotic arm and a gripper, which in total make the flying hand, and make it grasp either a static or a moving object. The main focus will be on verifying proper working of the controller throughout different system states: free-flight, docked to either a static object connected to a vertical wall or a dynamic one and fly away with an object. Lastly path tracking in the dynamic docked state will be verified which will require some added high level control of the system.

The stability of the control architecture is achieved by considering standard passivity-based feedback design techniques, where the stability of a desired equilibrium point is obtained by shaping the energy function of the system to have a desired minimum (*energy-shaping*), and then by dissipating energy to asymptotically converge to it (*damping-injection*). It will be shown that the complete system can be described by a cascade of these systems.

The main part of the research, i.e. the system analysis and control design, is presented as an article. Afterwards some conclusions will be drawn and recommendations given.

For the actual construction of the total aerial manipulation system a gripper that can be added to the robotic arm is required. The design hereof was done by reviewing several concepts by means of modelling. Afterwards one design is chosen and build. A full review of this process can be found in Appendix A.

The idea of attaching the object to another UAV was desired at first. Therefore the Ducted Fan UAV, designed by the University of Bologna was chosen. Its hardware and software needed to use the apparatus have been reviewed for this project and can be found in Appendix B. Unfortunately during the research the system was deemed not usefull at this stage for

this research due to the non-robustness of the system. For future reference however it is still included as an appendix to this report.

Modelling and Control of an Aerial Manipulation System with a Compliant Gripper

R.T.L.M. Tummers, M. Fumagalli and R. Carloni

***Abstract*— In this research, we present the design, simulation and experimental validation of a control architecture for an aerial manipulation system, i.e. a flying hand, that consits of an unmanned aerial vehicle, a robotic arm and a compliant gripper. The flying hand can realise mobile manipulation by grasping an object fixed to a vertical wall or a moving object that can exert dynamical forces. The goal of this work is to show that the overall control architecture allows the flying hand to approach the wall or the moving object, to dock on the object by means of the gripper and either detach the object from the wall or realise grasping and tracking of the mobile object in case of mobile manipulation. The control strategy has been implemented and validated in the simulated model as well as in experiments on the complete aerial manipulation system.**

I. INTRODUCTION

In recent years, the research interest in aerial service robots is increasing. One of the main goals is to use unmanned aerial vehicles (UAVs) in real application scenarios to support human beings in all those activities that require the ability to interact actively and safely with the environment not constrained to the ground, but indeed airborne [1]. Also interaction between UAVs plays a role as some tasks might require more than one UAV to accomplish them, e.g. carrying large and heavy objects.

Several works attest the interest in such challenging control scenarios. For instance, grasping and transportation using a fleet of quadrotors is considered in [2], and extended in [3] to assemble an infrastructure. The design of control architectures for the aerial manipulation of large objects using cables is considered in [4] and extended in [5]. In [6], a quadrotor helicopter is employed to clean a surface while hovering, where an additional propeller is employed to counteract contact forces while maintaining the stability of the vehicle. In [7], the physical interaction between a ducted fan aerial vehicle and the environment is considered. The approach considers to switch the control law in order to take into account for possible constraints deriving from the presence of contacts. Aerial grasping using an autonomous helicopter endowed with a manipulator is considered in [8] and [9]. In these cases, the analysis focuses on the stability of the vehicle during the interaction with a compliant environment. A prototype of miniature aerial manipulator has been proposed in [10].

This work has been funded by the European Commission's Seventh Framework Programme as part of the project AIRobots under grant no. 248669.

r.t.l.m.tummers@student.utwente.nl, {m.fumagalli,r.carloni}@utwente.nl, CTIT Institute, Department of Electrical Engineering, University of Twente, The Netherlands.

In this paper, we present the design, simulation and experimental validation of a control architecture for a flying hand and mobile manipulation with a moving object. The flying hand is composed of three different parts: a quadrotor UAV, a robotic arm and a gripper. The latter two combined is the robotic manipulator. The goal of the controller hereof is to show that the system can have three different operating states: free flight, docking on the object attached to a vertical surface, fly away with the object. In case of mobile manipulation the latter will be moving and exerting dynamical forces as well as impose a trajectory on the quadrotor UAV.

The stability of the control architecture is achieved by considering standard passivity-based feedback design techniques, where the stability of a desired equilibrium point is obtained by shaping the energy function of the system to have a desired minimum (*energy-shaping*), and then by dissipating energy to asymptotically converge to it (*damping-injection*).

The paper is organised as follows. In Section II, the overall mobile manipulation system is presented together with its dynamic model. In Section III, we propose the control strategy, which is validated in both simulations, in Section IV, and experimental tests, in Section V. Finally, concluding remarks are drawn in Section VI.

II. SYSTEM DYNAMICS

In order to design the control laws and analyse the stability of the flying hand while grasping an object, both fixed and in mobile manipulation, the overall model of the system dynamics is required. First, we discuss the structure of the complete system, secondly, each part is modelled individually.

A. System Overview

The complete gripper system is composed of three parts. The first is the underactuated quadrotor UAV, i.e. an AscTec Pelican quadrotor [11], as shown in Figure 1.

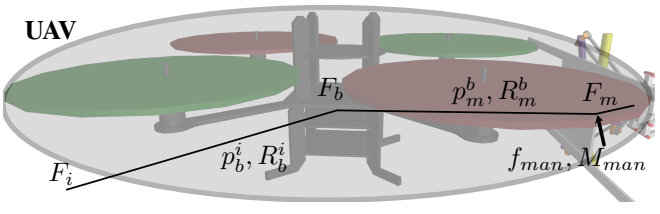

Fig. 1. The quadrotor UAV and its reference frames.

The second part is the robotic arm, based on a delta structure as introduced in [12]. This robotic arm consists of

a base plate, with three actuators and three legs (composed of a thigh and a shin parallelogram). It enables Cartesian movement in the workspace of its end-effector and can be used to track a certain point in the inertial frame regardless of the movements of the base plate, which is rigidly attached to the UAV.

Finally, the third part is an underactuated gripper, whose design is based on the work presented in [13]. The mechanical structure of the gripper consists of three fingers, with two phalanges each, and is actuated by one single motor. The construction of the gripper is such that form closure is guaranteed. The sketch of the robotic arm, the gripper and a fixed object is shown in Figure 2.

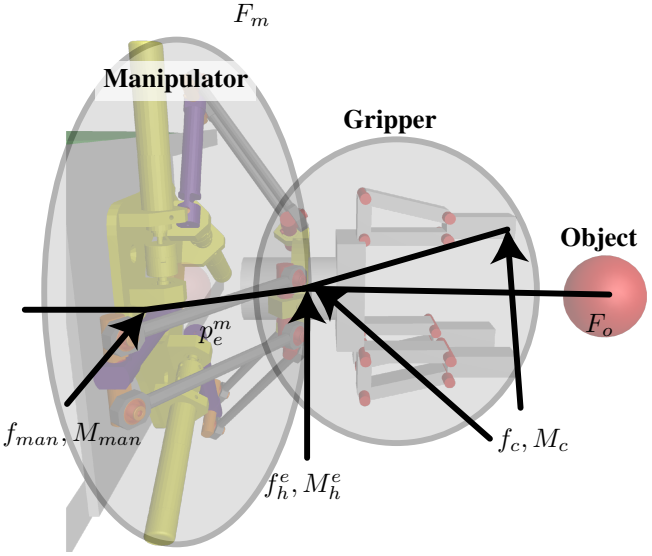

Fig. 2. The robotic manipulator, the gripper, the object and their reference frames.

For the case of mobile manipulation the object takes the form of a rod, to which the manipulator system can dock, connected to a wand that can exert forces on the system as well as impose a position.

B. Notation

Before proceeding with the description of the system dynamics, all used symbols are briefly explained for clarity. With reference to Figure 1 and Figure 2, the kinematic notation is:

- F_i, F_b, F_m, F_e, F_{f_i} and F_o, the inertial frame, the body frame of the quadrotor UAV fixed at its centre of gravity (c.g.), the base frame of the robotic arm, the base frame of the palm of the gripper (coincident with the base frame of the end effector of the robotic arm), the frame at the contact points on the fingers of the gripper and the object frame;
- $p_b^i = [x_b^i, y_b^i, z_b^i]^T$ and $R_b^i \in \mathbb{R}^{3\times3}$ the position and rotation matrix of the quadrocopter's c.g. with respect to the inertial frame, F_i;
- $p_m^b = [x_m^b, y_m^b, z_m^b]^T$ and $R_m^b \in \mathbb{R}^{3\times3}$ the position and rotation matrix of the robotic arm's base with respect to the frame at the quadrocopter's c.g., F_b;
- $p_e^m = [x_e^m, y_e^m, z_e^m]^T$ and $R_e^m \in \mathbb{R}^{3\times3}$ the position and rotation matrix of the palm of the gripper with respect to the robotic arm's base frame, F_m;
- $p_o^e = [x_o^e, y_o^e, z_o^e]^T$ and $R_o^e \in \mathbb{R}^{3\times3}$ the position and rotation matrix of the object with respect to the palm of the gripper;
- $p_{f_i}^o = [x_{f_i}^o, y_{f_i}^o, z_{f_i}^o]^T$ and $R_{f_i}^o \in \mathbb{R}^{3\times3}$ the position and rotation matrix of each of the contact points i of the gripper's fingers with respect to the object frame, F_o; $\boldsymbol{r}_{f_i}$

The dynamic notation is:

- g the gravitational acceleration;
- m_{uav}, J_{uav} are the quadrotor UAV's mass and inertia matrix;
- $f_p^b \in \mathbb{R}^3$ the total thrust on the quadrocopter generated by its propellers, $f_{man}^m \in \mathbb{R}^3$ the force the robotic arm and the UAV exert on each other at the robotic arm's base;
- $M_{gy}^b \in \mathbb{R}^3$ the moment vector due to the gyration effects of the propellers of the quadrocopter, $M_p^b = [M_x, M_y, M_z]^T \in \mathbb{R}^3$ the control torque of the vehicle, $M_{man}^m \in \mathbb{R}^3$ the reaction torque the robotic arm and the UAV exchange at the robotic arm's base;
- $f_{I_m}^m, M_{I_m}^m \in \mathbb{R}^3$ the vectors of all the dynamical forces and moments due to the absolute motion of the robotic arm in F_m;
- $f_{I_h}^e, M_{I_h}^e \in \mathbb{R}^3$ the vectors of all the dynamical forces and moments due to the absolute motion of the compliant gripper in F_e;
- $f_h^e, M_h^e \in \mathbb{R}^3$ the force and moment vectors the gripper and the robotic arm's end-effector exert on each other;
- $f_{obj}^o, M_{obj}^o \in \mathbb{R}^3$ the force and moment vectors that make up the total wrench, w_{obj}, the object exerts on the gripper's fingers and palm in the object frame, F_o;
- $f_p^b = [x_p^b, y_p^b, z_p^b]^T \in \mathbb{R}^3$ the total thrust on the ducted fan generated by its propeller and vanes;
- $M_{gy}^d \in \mathbb{R}^3$ the moment vector due to the gyration effects of the propeller of the ducted fan, $M_p^d = [M_x, M_y, M_z]^T \in \mathbb{R}^3$ the control torque of the vehicle.

From a dynamical point of view, the complete system is seen as a cascade of subsystems, interconnected at certain points by means of localised interaction forces and moments. It is assumed that the system interacts with the environment (i.e. a static object or a mobile one) by means of the gripper's base and the phalanges only, i.e. only in F_e and F_f. Furthermore, the connections between the UAV and the robotic arm's base in F_m as well as between the robotic arm's end-effector and the gripper's palm in F_e are assumed to be rigid. The quadcopter UAV itselve in F_b is unconstrained and can thus move freely with respect to the inertial frame, F_i.

C. The Quadrotor Dynamics

The quadrotor is an underactuated system, since it has only four control inputs f_i, i.e. its propellers, and six degrees of freedom (DoF). Due to the mechanical design of the quadrotor, a net torque can be applied in any direction by varying the relative thrust of the propellers. The mapping

between the generated force of each propeller and the total thrust and torque exerted on the quadrotor UAV's c.g. is given by

$$\begin{bmatrix} f_p^b \\ M_x \\ M_y \\ M_z \end{bmatrix} = \begin{bmatrix} 1 & 1 & 1 & 1 \\ 0 & -d & 0 & d \\ d & 0 & -d & 0 \\ -c & c & -c & c \end{bmatrix} \begin{bmatrix} f_1 \\ f_2 \\ f_3 \\ f_4 \end{bmatrix} \quad (1)$$

where d is the distance between the quadrotor UAV's c.g. and the centre of the propeller, and c is the ratio between the propeller reaction torque and generated thrust. Using this, the full dynamics of the quadrotor UAV can be described by

$$\begin{aligned} m_{uav}\dot{v}^i &= m_{uav}g\hat{z}^i + f_p^b R_b^i [0,0,-1]^T + R_b^i R_m^b f_{man}^m \\ J_{uav}\dot{\omega}_b^{b,i} &= -\omega_b^{b,i} \times J_{uav}\omega_b^{b,i} + M_{gy} + M_p^b \\ &\quad + R_m^b M_{man}^m + R_m^b f_{man}^m \times p_m^b \end{aligned} \quad (2)$$

where $\dot{\omega}_b^{b,i}$ and $\omega_b^{b,i}$ are the rotational velocity and acceleration of the quadrotor UAV with respect to F_i expressed in F_b, respectively; $\dot{v}^i$ the linear acceleration of the quadrotor UAV's c.g. in F_i.

D. The Robotic Arm Dynamics

The dynamics of the robotic arm can be compactly described by dividing them into the internal and external dynamics. The former includes inertial and gravitational contributions as well as the dynamic influence of the actuators. The latter upholds forces and moments exchanged at the end effector with the gripper and due to interaction with the environment. From the equilibrium of forces and moments the dynamics of the robotic arm in F_m are described by:

$$\begin{aligned} f_{man}^m &= f_{I_m}^m + R_e^m f_h^e \\ M_{man}^m &= M_{I_m}^m + R_e^m M_h^e + R_e^m f_h^e \times p_e^m \end{aligned} \quad (3)$$

E. The Gripper Dynamics

The dynamics of the gripper are similar to the dynamics of the robotic arm. The dynamic contributions can be divided into internal and external, i.e. the gripper is attached at the robotic arm's end-effector and is the source of all forces and moments exchanged here. Also the gripper can be loaded by an external force, given by the interaction with the object. Therefore, the dynamics of the gripper can be described by

$$\begin{aligned} f_h^e &= f_{I_h}^e + R_o^e f_{obj}^o \\ M_h^e &= M_{I_h}^e + R_o^e M_{obj}^o + R_o^e f_{obj}^o \times p_o^e \end{aligned} \quad (4)$$

F. The Environment

The system is allowed to be in three different states: free-flight (no object), docking (on the object) and aerial grasp (with object). Therefore, both f_{obj}^o and M_{obj}^o in Equation 4 can have three different interpretations, depending on which state the system is in. These three states and their influence on the system are explained hereafter.

1) Free-flight state (no object): In this state, the UAV is in free flight and no object is grasped. This results in no external force and moment, i.e.,

$$\begin{aligned} f_{obj}^o &= 0 \\ M_{obj}^o &= 0 \end{aligned} \quad (5)$$

2) Docking state (on the object): In this state, the quadrotor UAV is docked on the object and, more precisely, it is docked by means of the gripper that is grasping the object attached to a vertical surface. The reaction forces and moments are partly due to the contact between the object and the base of gripper and partly due to the interaction between the object and the phalanges of the gripper. These forces and moments are described by

$$[f_{obj}^o, M_{obj}^o]^T = G f_c \quad (6)$$

where G is the grasp matrix consisting of the rotational matrices and translational vectors of all the contact points and

$$f_c = [f_c^{f_1}, f_c^{f_2}, f_c^{f_3}, f_c^{f_4}, f_c^{f_5}, f_c^{f_6}, f_c^p]^T \quad (7)$$

is the net vector of the contact forces. The contacts are modelled as a point contact with friction [14]. Here each contact force consists of a normal force which is modelled by the Hunt-Crossley model [15] and two tangential friction components, which are a fraction of the normal force.

3) Aerial grasp state (with object): When the object is detached from the vertical wall, it becomes part of the complete system. Therefore, since the only net force acting on the object is gravity, the dynamic contribution of the object becomes

$$[f_{obj}^o, M_{obj}^o]^T = [0,0,m_{obj}g,0,0,0]^T \quad (8)$$

III. CONTROL

In this section, we divide the total system into several cascaded impedance controlled subsystems. For clarity, each subsystem will be handled separately.

A. The Quadrotor UAV

Assuming a high attitude control authority like in [16], that compensates momenta imposed on the system, the quadrotor UAV's system dynamics in Equation 2 can be reformulated to

$$m_{uav}\dot{v}^i = m_{uav}g\hat{z}^i + f_p^b R_b^i [0,0,-1]^T + R_b^i R_m^b f_{man}^m \quad (9)$$

where $R_b^i R_m^b f_{man}^m$ are the forces the robotic manipulator exerts on the quadrotor UAV.

The only controllable input is $f_p^b R_b^i [0,0,-1]^T$. In order to compensate for gravity, this is chosen to be

$$f_p^b R_b^i [0,0,-1]^T = u - m_{uav}g\hat{z}^i \quad (10)$$

with $u = [u_x, u_y, u_z] \in \mathbb{R}^3$ as a new input. Substituting this into Equation 9 results in

$$m_{uav}\dot{v}^i = u + F_{ext}(t) \quad (11)$$

in which $F_{ext}(t) = R_b^i R_m^b f_{man}^m(t)$. Note that the system now resembles a mass driven by an external force and an other input, that still has to be defined.

Now let p_b^{*i} be the desired position for the aerial vehicle. By choosing u to be equal to

$$u = -K_p(p_b^i - p_b^{*i}) - K_d v^i \tag{12}$$

the system becomes impedance controlled. Here K_p and K_d can be chosen according to the desired system bandwidth and relative damping. It should be noted that the overall mass of the system, m_{uav}, changes when the object is grasped and detached from the vertical wall. This means that the mass compensation part of the control law also has to change.

B. The Robotic Arm

In its essence the control of the robotic arm is similar to the control of the quadrotor UAV. The only difference is the way that the inputs map to the robotic arm's end effector position, which is described by the Jacobian of the Delta structure.

By working out the summation of internal forces, $f_{I_m}^m$, in Equation 3, under the assumption that all the mass is concentrated on the end-effector, the following is obtained

$$f_{man}^m = m_{total} g \hat{z}^i + f^m - m_{total} R_e^m \dot{v}^e + R_e^m f_h^e \tag{13}$$

in which f^m is the force on the end-effector frame delivered by the motors that drive the legs of the Delta structure, $\dot{v}^e$ is the end effector acceleration and $m_{total} = m_{delta} + m_{gripper} + m_{obj}$, where m_{obj} is only non-zero in the *aerial grasp state*.

If the controllable input part is chosen to be

$$f^m = u - m_{total} g \hat{z}^i \tag{14}$$

with $u = [u_x, u_y, u_z] \in \mathbb{R}^3$ as a new input and substituting this in Equation 13, the following is obtained

$$m_{total} R_e^m \dot{v}^e = u + F_{ext}(t) \tag{15}$$

in which $F_{ext}(t) = R_e^m f_h^e(t) - f_{man}^m(t)$.

Once again the dynamics of this subsystem resemble a mass driven by an external force. Therefore, the same manner of control as the UAV can be applied. Let a desired virtual point be represented by p_e^{*i} and define u as

$$u = -K_p(p_e^m - p_e^{*m}) - K_d v^e \tag{16}$$

which turns this system into an impedance controlled one.

C. The Gripper

In order to fulfill the requirement that the overall system should consist of impedance controlled subsystems, we have to design the control for the gripper in a similar manner as the previous subsystems.

Before that, it should be noted that the only interesting state from a control point of view is the docking state, since in both other states the gripper is either idle in its open state or idle in a closed state.

Expanding the internal forces, $f_{I_h}^e$ in Equation 4 for this state, results in

$$f_h^e = f_{grav} + r_{pul}\tau^m - m_{phals} R_o^e G \dot{v}_{phals}^f + R_o^e f_{grasp}^o \tag{17}$$

where r_{pul} is the radius of the output pulley, τ^m the motor torque, m_{phals} a diagonal matrix with the masses of all the individual phalanges, $\dot{v}_{phals}^f$ a column vector with the acceleration of each of the phalanges and f_{grasp}^o the force part of the result of Gf_c.

Under the assupmtion that f_{grav} is negligible due to the low weight of the phalanges, this equation can be rewritten as

$$m_{phals} R_o^e G \dot{v}_{phals}^f = u + F_{ext}(t) \tag{18}$$

with $F_{ext}(t) = R_o^e f_{grasp}^o - f_h^e$ and u a yet to define control input. By letting u be

$$u = -K_p(p_f^e - p_f^{*e}) - K_d v_f^e \tag{19}$$

with p_f^{*e} the desired position of the gripper's fingers, the subsystem becomes impedance controlled.

It should be noted that as the gripper is an underactuated system, there is only one actuator to actuate three fingers with two phalanges each. This implies that the pseudoinverse of the grasp matrix G should be computed, e.g. by means of a MoorePenrose pseudoinverse, in order to calculate p_f^e and v_f^e.

However since the used gripper is compliant, the positions and orientations of all the phalanges is not fully deterministic. Therefore actual knowledge to calculate the inverse is missing.

Another thing to not is the fact that actual gravity compensation by means of control is impossible due to the opposing fingers and therefore opposing gravity vectors.

D. Stability analysis

Under the assumption that the force of gravity on the phalanges is indeed negligible, all the subsystems have the same generalized closed loop system;

$$m\dot{v}^j + K_d v^j + K_p(p^j - p^{*j}) = d \tag{20}$$

with $v^j = \dot{p}^j$. Here j denotes the frame that corresponds to the subsystem. Therefore a single stability analysis will suffice. In fact the described system turns out to be *output strictly passive* [17] by choosing input d, output v^j and storage function

$$V(v^j, p^j) = K(v^j) + P(p^j) \tag{21}$$

where $K(v^j)$ denotes the kinetic energy, given by

$$K(v^j) = \frac{1}{2} m (v^j)^T v^j \tag{22}$$

and $P(p^j)$ is the potential energy, given by

$$P(p^j) = \frac{1}{2}(p^j - p^{*j})^T K_p (p^j - p^{*j}) \tag{23}$$

which has a minimum at the desired position p^{*j}. As shown in [17][Lemma 6.7] the above property of *output strict passivity* can be linked to zero-input asymptotic stability via zero-state observability and can be shown to hold for the generalized dynamics of the subsystems in Equation 20.

This means that all the subsystems asymptotically reach the desired setpoints, denoted p^{*j} in Equation 20, provided their input forces are zero.

Due to the cascaded nature of the subsystems and the fact that all of the subsystems are asymptotically stable, the overall system is also asymptotically stable [18].

E. High level control

For the aerial manipulation test some high level control is needed, specifically when the flying hand is docked moving object. In order to create some kind of tracking capabilities in this state the desired positions of the quadrotor UAVs should be coupled to the object's. This is done in such a way that the desired distance between the two remains constant, i.e. the quadrotor UAV's reference position becomes dependend on the position of the wand.

IV. SIMULATIONS

In this section, we show the simulation results in order to validate the proposed control strategy.

A. Simulations

At first the flying hand is simulated with a fixed object. In order to do so, the model is implemented in the simulation package 20-sim [19]. By simulating the model, it can be shown that stable flight and stable interaction can be achieved.

Secondly the fixed object is interchanged with the bar shaped object connected to the wand and a similar simulation is performed. This includes a path tracking experiment where the flying hand is docked to the wand.

1) Quadrotor UAV path tracking: Figure 3 shows the simulation results for the quadrotor UAV's position while tracking a certain path. The denotion *setpoint* corresponds to desired position denoted p^{*j} in Equation 20.

Note that all three operating states are shown sequentially. At the beginning, the quadrotor UAV is in its *free-flight state (no object)*. Upon contact with the object at $t = 6.7$ s, the system is in its *docking state (on the object)*. When the object is fully grasped and the quadrotor UAV flies away from the wall at $t = 11$ s, the object is detached from the vertical wall and becomes a part of the complete system. The system is finally in its *aerial grasp state*.

As shown in Figure 3, the quadrotor UAV is capable of tracking the path in all the states. Some tracking errors are present, due to impedance control. Also some larger fluctuations can be seen when the system is in contact with the environment, still stability is guaranteed. Note that the tracking error converges to zero when the setpoint is constant for a sufficient amount of time. This is in accordance with the stability analysis in Subsection III-D.

2) Robotic arm path tracking: In order to asses the correct functioning of the robotic arm, the tracking capabilities with respect to the robotic arm's base frame, F_m, is shown in Figure 4.

Note that object tracking is disabled for $t < 6$ s as there is no need to track any object yet. Enabling object tracking would only result in unnecessary disturbances on the system. At $t = 10$ s, the object tracking is disabled again as this is no longer useful when the object is detached from its surroundings.

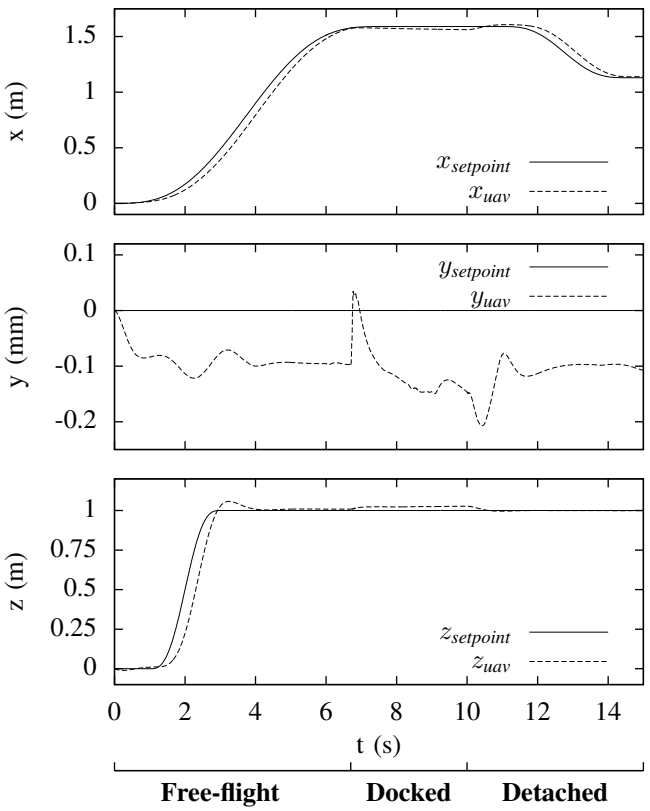

Fig. 3. Path tracking of the quadrotor UAV with respect to the inertial frame F_i. The visible offset in y is most likely due to the slight off centre weight of the robotic arm.

From Figure 4 it can be seen that the tracking capabilities of the Delta structure prove to be sufficient to retain a stable system. Note that larger fluctuations occur when the system is in contact with the environment, but the tracking and the overall stability are still guaranteed. The spikes at the time of impact are due to the displacement of the UAV on impact, as seen in the middle plot in Figure 3. The sudden change in $x_{setpoint}$, which is the height with respect to F_m, can be caused by the contact friction and by the fact that the quadrotor is not yet stabilised.

3) Dynamical Object Path Tracking: In order to verify object tracking capabilities with a moving object, the simulations were altered slightly. The static round object was replaced by a bar-shaped object whos position could be controlled. Its imposed reference position is set as a reference for the quadrotor UAV and robotic arm as well, with some offset of course, when it has come close enough to the object, which was set to be at $t = 10$ s. After this the object tracks a closed path in the x-z plane for 20 s after which the simulation comes to an end. The results of these simulations can be found in Figure 5, Figure 6 and Figure 7.

The position of the wand, although not plotted here, is

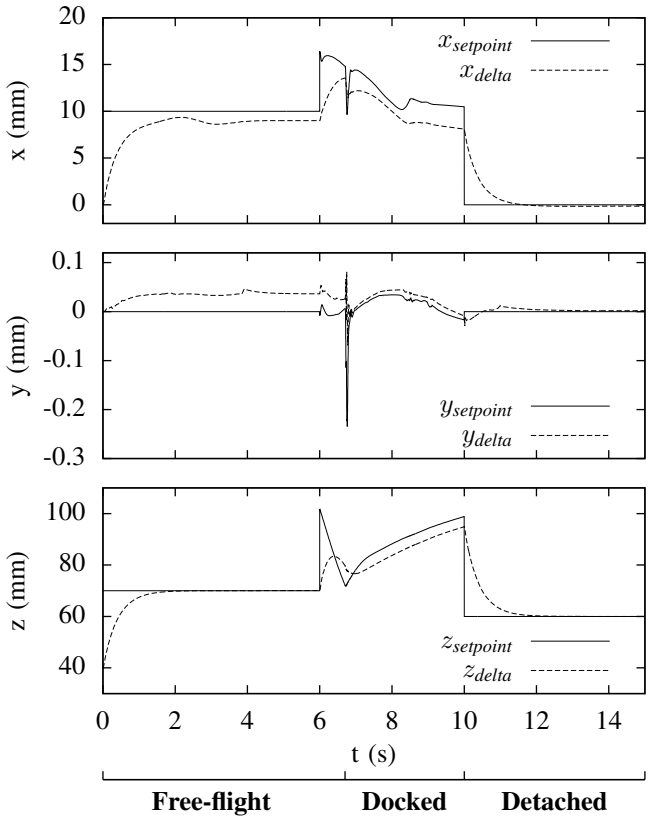

Fig. 4. Path tracking of delta structure with respect to manipulator base frame F_m.

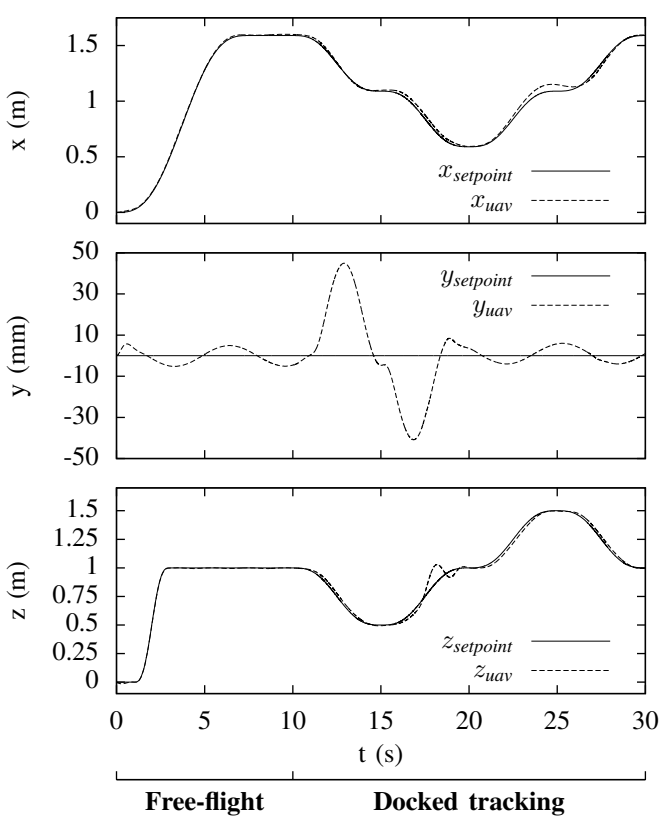

Fig. 5. Path tracking of the quadrotor UAV with respect to the inertial frame F_i. The visible offset in y is partly due to the added disturbance and probably also partly due to the fact that the object is not grasped completely in its centre of mass.

similar to the reference position of the quadrotor UAV from $t = 10\ s$ onwards, before this the reference is just constant so the object remains in the same location. The position itself is simulated by imposing a path on the object through a PD controller in order to resemble human motion.

It should be noted that there is also some external force applied to the system in order to simulate external disturbances like wind gusts. These are chosen to be periodic in nature, since this seemed to resemble the observed disturbances to the real system.

Stable flight in both free-flight and docked tracking states can be observed in Figure 5. However a slightly higher offset than desired can be observed at $t = 18\ s$, that is hard to explain. It might be due to interference of the imposed path and the generated external disturbance on the system.

In Figure 6 proper compensation for the offset of the quadrotor UAV with respect to its reference can be observed. This can specifically be seen when comparing the y-plots of this figure with Figure 5 as they show a remarkable anti-symmetry and thus full compensation for the offsets.

Lastly Figure 7 shows the tracking of the quadrotor UAV in the x-z plane for $t = [10, 30]\ s$. This also shows that the proposed system seems to handle proper object tracking and stability throughout this stage.

Based on the simulation results as shown above, the system looks stable in theory. Experiments have to proof this also holds in practice.

V. EXPERIMENTS

In this section experimental validation of the proposed control architecture will be handled for both a static and a moving object.

A. Experimental setup

In order to verify the proposed control strategy, a test setup has been build together with a software architecture as seen in Figure 8. All the different modules will briefly be presented hereafter:

- Quadrotor UAV: an AscTec Pelican quadrotor, weighing 750 grams and capable of handling a payload of 500 grams [11]. The low level attitude control of the vehicle is performed onboard by two ARM7 microprocessors. An additional Intel Atom 1.6 GHz processor performs the position control of the aerial platform
- Robotic arm: a 3 DoF cartesian delta robotic manipulator as proposed in [12]. The control of this system runs on an Arduino ATMega2560 and it receives setpoints by the ground station by means of a WiFi data link.
- Compliant gripper: a 3D printed gripper system consisting of three fingers with two phalanges each. The system is actuated by one motor attached to the aerial vehicle and connected via bowden cables to the gripper in order to minimise the UAV's inertia. The motor itself is controlled by the microcontroller on the Arduino.

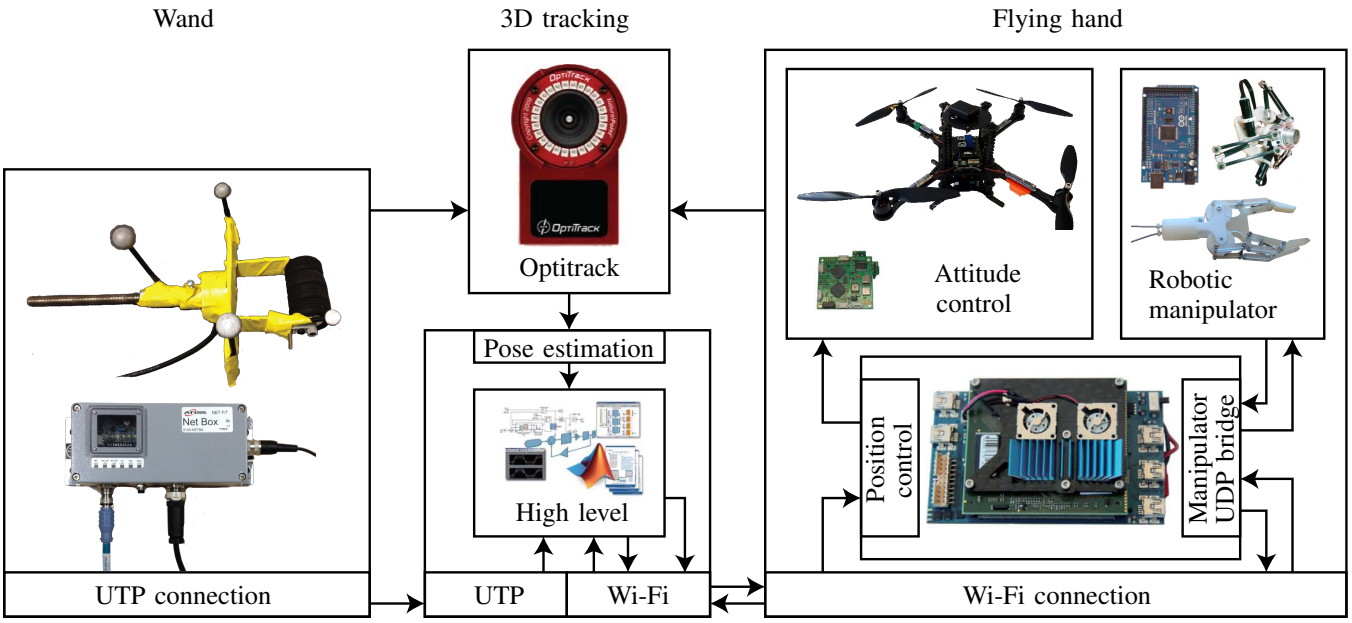

Fig. 8. The overall system used for experiments. Note that the left most part (Wand) is not used for the first experiment.

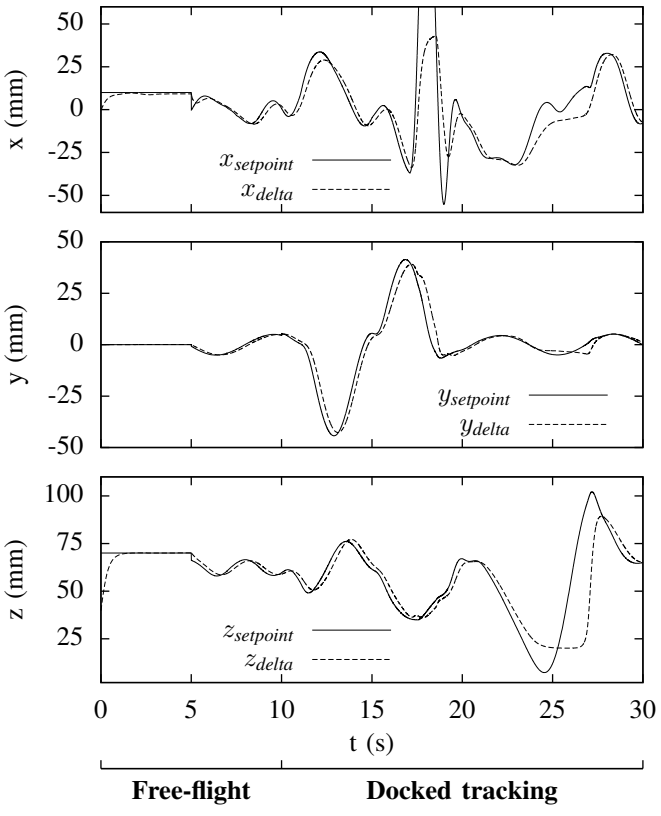

Fig. 6. Path tracking of the robotic arm with respect to manipulator base frame F_m. Overall the subsystem seems to do what it is supposed to, altough some hard to explain offsets occur around $t = 25$ s. This might be due to a fast change in reference position.

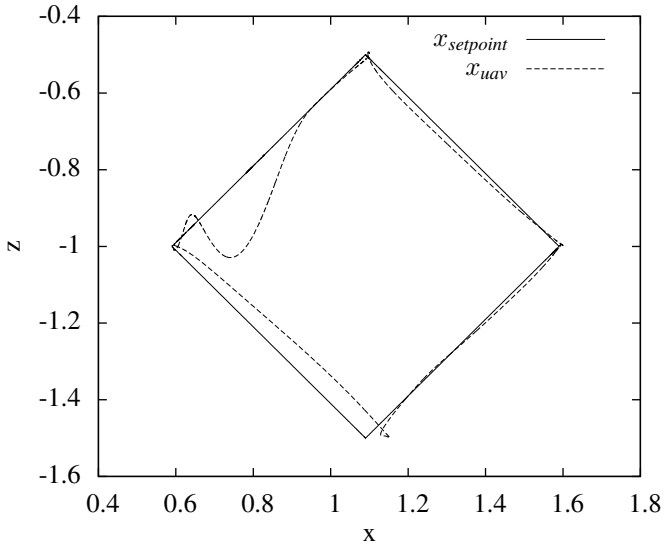

Fig. 7. Path tracking of the quadrotor UAV in the x-z plane for $t = [10, 30]$ s. It shows proper tracking and also the before mentioned larger offset.

- An object, which is a small foam ball for the first experiment and a wand, consisting of a force sensor and a bar shaped object, for the second experiment.
- External positioning system: the positions of the subsystems in the inertial frame, F_i, are estimated by an external optical tracking system OptiTrack Flex 13. [20], which allows tracking by placing passive markers on the subsystems.
- Ground station: the high-level controller of the system, i.e. it generates trajectories and estimates positions based on the input of the OptiTrack, and runs on Ubuntu Linux 10.10. The communication between the different software modules is performed using the Robot

Operating System (ROS) framework [21]. Setpoints generated for both the robotic arm and the gripper are relayed to the integrated microcontroller via WiFi (802.11n standard).

B. Experiment validation

This subsection is divided into two parts. The first part shows the results of an experiment with an object statically connected to a wall. Thereafter a second experiment with a moving object is handled.

1) Static object: The first experiment is aimed at validating safe and robust operation of the system throughout the three different object states.

In order to perform the experiments the robotic manipulator approaches the object in the inertial frame. In order to achieve that, the desired pose of the robotic manipulator can be derived by the measured UAV's position and the desired point on the vertical wall. Once the UAV is in front of the object, the gripper grasps the object, detaches it from the wall and flies away with the object.

Figure 9 shows that the UAV is capable of tracking the given setpoints through all three states. The UAV starts in free-flight and, at approximately 30 s, grasps the object. A few seconds later the object is removed from the vertical wall leaving the UAV in free-flight mode with the object still attached.

Some notes should be placed on the measured values for the y-position, which is the sideway motion of the UAV. Compensation in this direction is difficult due to the underactuated nature of the UAV. Moreover, the noise is caused by the turbulence generated by the propellers in the small indoor environment. The fact that the object is connected to a wall amplifies this effect even more. This also causes the robot to drift away once before grasping the object.

During the experiment the robotic manipulator tracks its setpoint the entire time. This can clearly be seen in Figure 10 since the z- and x-position are almost in their outmost position (i.e. 120 mm for z and 50 mm for x).

At $t = 30$ s the inertial position tracking is clearly visible as the peaks in both the y- and z-setpoints. After grasping, the robotic manipulator keeps on tracking the given setpoint which causes it to move outward again, but now with a grasped object. Good tracking performance and stability can be observed.

2) Moving object: The aim of the moving object experiment is to verify that the system behaves in a safe and robust manner. To accomplish this external forces are exerted on the system by means of a wand like object that can be operated by a human being. Attached to the wand is a bar shaped object that can be gripped by the robotic manipulator. Also an attached force sensor gives insights into the exerted force on the system by the human.

Next to verification of the robustness to external forces, the wand is also used to impose a position on the UAV, i.e. they will move cooperatively. Therefore the position of the wand is also tracked and when within a certain range, i.e.

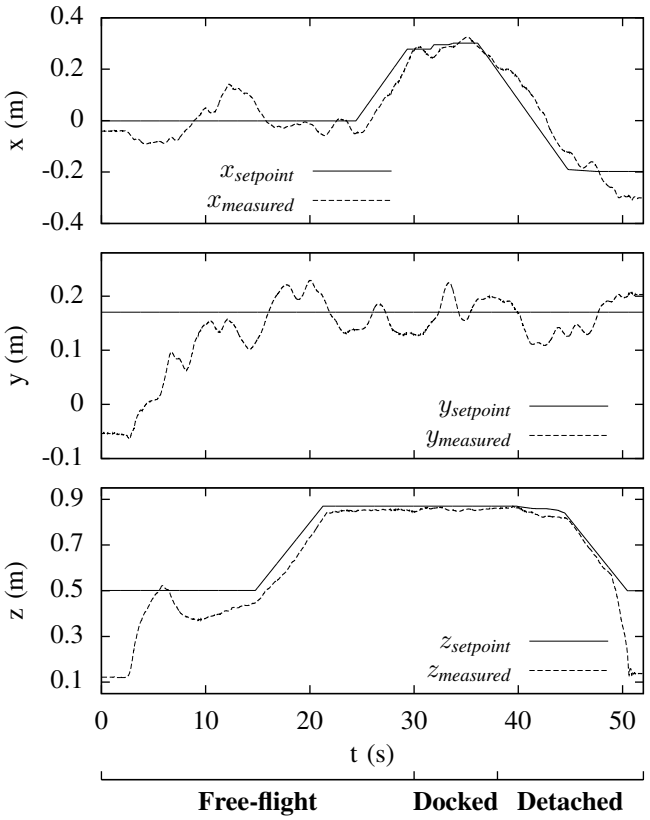

Fig. 9. Path tracking of the quadrotor UAV with respect to the inertial frame, F_i. x denotes the forward direction, y the sideward direction and z the height of the quadrotor UAV. Good tracking performance can be observed, although some external influences, due to the wind gust, are clearly visible.

the offset to its desired position with respect to the UAV is within -5 and 35 cm for x and -20 and 20 cm for both y and z, of the UAV imposed onto the UAV as well with an experimentally determined predefined desired offset to the wand. In the results shown the wand is already within this region. At the end of the experiment when the wand leaves this region, the last given setpoint is retained, leaving the UAV to hover steadily. This can be observed in Figure 11.

For this experiment the robotic manipulator is configured such that it always tries its best to follow the wand.

Reviewing Figure 11 the quadrotor UAV shows stable flight for both free-flight and docked tracking modes. It does show some offset with respect to the setpoints, but these are perfectly compensated for by the robotic arm as can be seen in Figure 12. It should be noted that the robotic arm has to use almost its entire workspace to accomplish this, therefore we might say that it is almost at its maximum capacity in terms of compansation.

To overcome the capacity problem, it might be useful to make the position control of the quadrotor UAV more aggressive, i.e. stiffer. However this should be explored with care as this might make the system unstable.

Another observation can be done when reviewing the results in Figure 12. The graphs are rather noisy compared to those of the quadrotor UAV. This is most likely due to

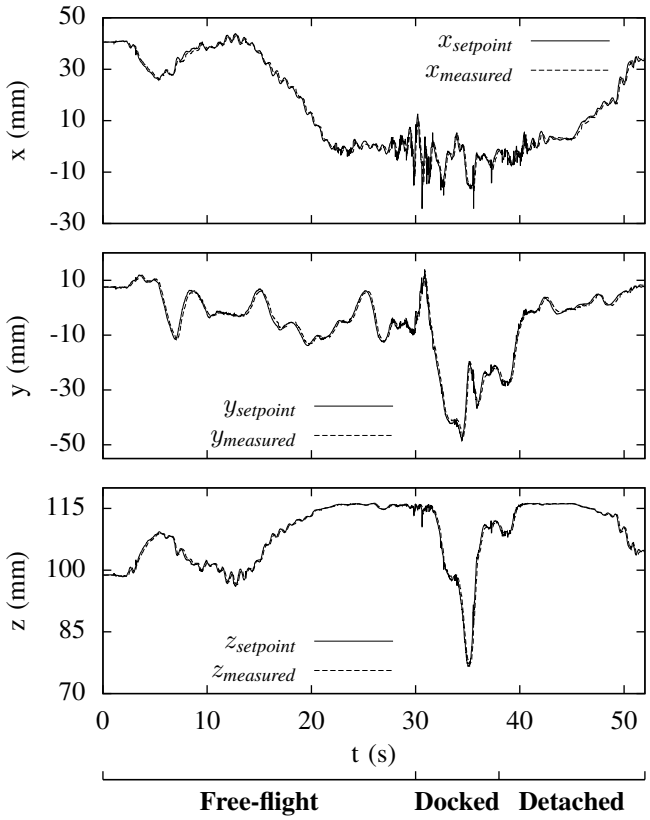

Fig. 10. Path tracking of the end effector of the delta structure with respect to the base frame of the delta structure, F_b. x denotes the height of the manipulator, y denotes the sideways movement and z denotes the forward motion.

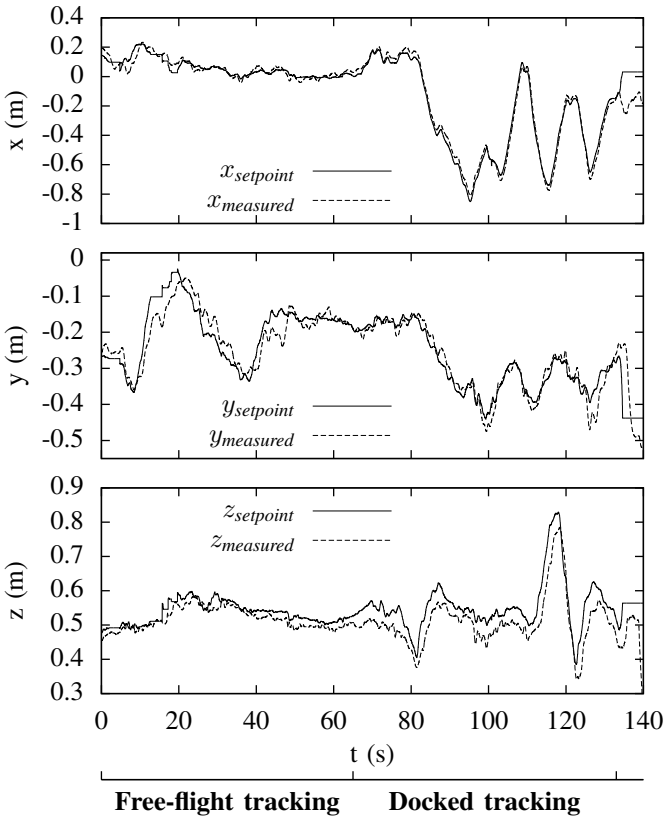

Fig. 11. Path tracking of the quadrotor UAV with respect to the inertial frame, F_i. x denotes the forward direction, y the sideward direction and z the height of the quadrotor UAV. Good tracking performance can be observed, both during free-flight tracking of the wand, docked tracking and idle free-flight.

the fact that the reference position for the robotic arm is calculated based on two measured positions, i.e. the wand and the quadrotor UAV. Accuracy of and fluctuations in these measured positions are therefore reflected more in this reference. Next to that results the actuation of the robotic arm in an impuls on the quadrotor UAV as well.

Next to that there are also several sources of delay in the system, e.g. the OptiTrack visual tracking system and the communication between the PC running the control code and the quadrotor UAV.

For clarity the position of the wand in the inertial frame, F_i, can be seen in Figure 13. This figure also shows the forces that the human exerts on the aerial manipulator through the wand. Part of this force is absorbed by the robotic manipulator which behaves like a buffer between the external force input and the quadrotor UAV.

Apart from that the graphs clearly show that the system is able to handle forces more than 2 N in a single direction. Calculation of the norm for each measurement shows that the system can even handle forces over 3 N.

Lastly Figure 14 shows both an x-y and an x-z plot of the path tracking capabilities of the quadrotor UAV when docked. This also shows that the quadrotor UAV is not always capable of following the reference closely. However it remains stable and due to the robotic manipulator in contact with the wand.

VI. Conclusions

In this paper, we presented the design of a control architecture for a flying hand and a mobile manipulation system. The flying hand consists of an unmanned aerial vehicle, a robotic manipulator and a gripper, which is grasping an object fixed on a vertical wall or a mobile one, attached to a wand controlled by a human. The control strategy is based on passivity-based techniques and has been shown to guarantee the asymptotic stability of the system in both simulations and in experimental tests.

References

[1] AIRobots. [Online]. Available: http://www.airobots.eu

[2] D. Mellinger, M. Shomin, N. Michael, and V. Kumar, "Cooperative grasping and transport using multiple quadrotors," in *Proceedings of the International Symposium on Distributed Autonomous Robotic Systems*, 2010.

[3] Q. Lindsey, D. Mellinger, and V. Kumar, "Construction of cubic structures with quadrotor teams," in *Proceedings of the Robotics: Science and Systems Conference*, 2011.

[4] N. Michael, S. Kim, J. Fink, and V. Kumar, "Kinematics and statics of cooperative multi-robot aerial manipulation with cables," *University of Pennsylvania, USA, Technical Report*, 2009.

[5] Q. Jiang and V. Kumar, "The inverse kinematics of 3-d towing," *Advances in Robot Kinematics: Motion in Man and Machine*, pp. 321–328, 2010.

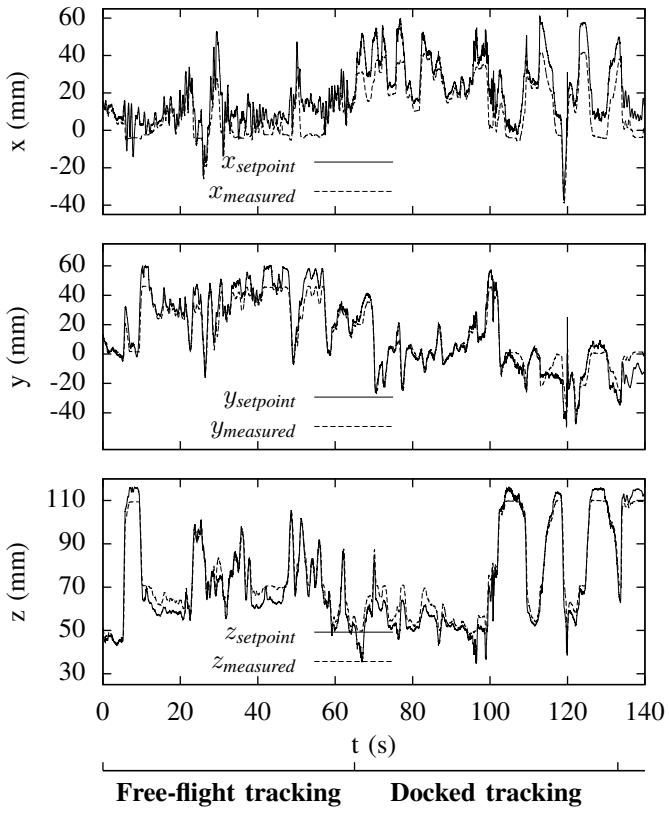

Fig. 12. Path tracking of the end effector of the delta structure with respect to the base frame of the delta structure, F_b. x denotes the height of the manipulator, y denotes the sideways movement and z denotes the forward motion away from the quadrotor UAV. Note that almost the whole workspace of the manipulator is used to compensate for the UAV's offset to the setpoint as seen in Figure 11.

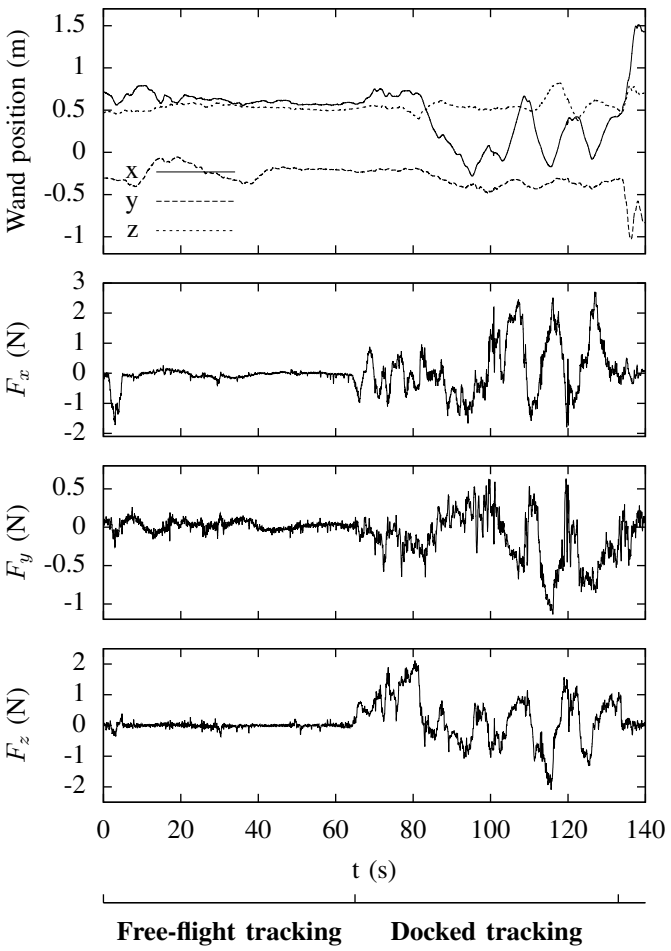

Fig. 13. Measured path of the wand (top) as well as the forces exerted by the wand on the manipulator system (bottom three).

[6] A. Albers, S. Trautmann, T. Howard, T. Nguyen, M. Frietsch, and C.Sauter, "Semi-autonomous flying robot for physical interaction with environment," in *Proceedings of the IEEE Conference on Robotics Automation and Mechatronics*, 2010.

[7] L. Marconi, R. Naldi, and L. Gentili, "Modeling and control of a flying robot interacting with the environment," *Automatica*, vol. 47, no. 12, pp. 2571 – 2583, 2011.

[8] P. Pounds, D. Bersak, and A. Dollar, "Grasping from the air: hovering capture and load stability," in *Proceedings of the IEEE International Conference on Robotics and Automation*, 2011.

[9] P. Pounds and A. Dollar, "UAV rotorcraft in compliant contact: Stability analysis and simulation," in *Proceedings of the IEEE/RSJ International Conference on Intelligent Robots and Systems*, 2011.

[10] C. Korpela, T. Danko, and P. Oh, "MM-UAV: Mobile manipulating unmanned aerial vehicle," *Journal of Intelligent & Robotic Systems*, vol. 65, no. 1–4, pp. 93–101, 2012.

[11] "Ascending Technologies." [Online]. Available: http://www.asctec.de/

[12] A. Keemink, M. Fumagalli, S. Stramigioli, and R. Carloni, "Mechanical design of a manipulation system for unmanned aerial vehicles," in *Proceedings of the IEEE International Conference on Robotics and Automation*, 2012.

[13] G. A. Kragten, "Underactuated hands - fundamentals, performance analysis and design," Ph.D. dissertation, TU Delft, 2011.

[14] R. Murray, Z. Li, and S. Sastry, *A mathematical introduction to robotic manipulation*. CRC, 1994.

[15] N. Diolaiti, C. Melchiorri, and S. Stramigioli, "Contact impedance estimation for robotic systems," *IEEE Transactions on Robotics*, vol. 21, no. 5, pp. 925–935, 2005.

[16] M. Fumagalli, R. Naldi, A. Macchelli, R. Carloni, S. Stramigioli, and L. Marconi, "Modeling and control of a flying robot for contact inspection," in *Proceedings of the IEEE/RSJ International Conference on Intelligent Robots and Systems*, 2012.

[17] H. K. Khalil, *Nonlinear Systems*. Prentice Hall, 1996.

[18] N. Hogan, "Impedance control: An approach to manipulation," *Journal of Dynamic Systems, Measurement, and Control*, vol. 107, no. 1, pp. 1 – 24, 1985.

[19] "20sim." [Online]. Available: http://www.20sim.com

[20] "OptiTrack." [Online]. Available: http://www.naturalpoint.com/optitrack/

[21] "ROS. Robot Operating System." [Online]. Available: http://www.ros.org

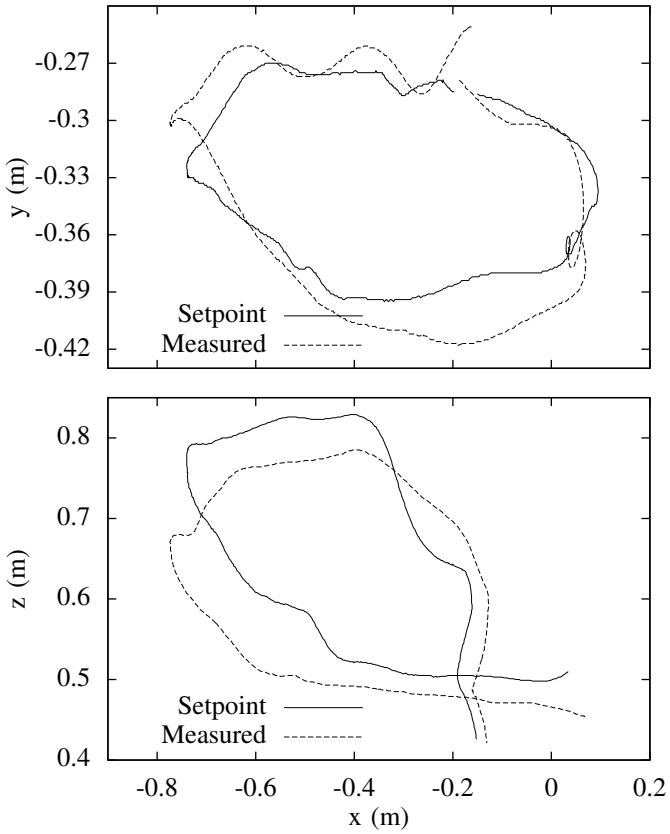

Fig. 14. Path tracking of the quadrotor UAV with respect to the inertial frame, F_i, both in the x-y and x-z plane. This data corresponds to $t = [107, 120]$ for the former and $t = [110, 122]$ for the latter of the data in Figure 11.

Conclusions

The work presented in this research showed the design of a control architecture for a flying hand as well as a mobile manipulation system. Herein the flying hand is composed of three subsystem; a quadrotor UAV, a robotic manipulator and a gripper. For mobile manipulation a wand like object was added to the system. This want had to be operated by a human being and allowed for some insights into the interaction forces.

The proposed control architecture, a cascade of impedance controlled subsystems, was shown to guarantee the asymptotic stability of the system in theory, simulation as well as experiment for different states, i.e. free-flight, docking to both a static and a dynamical object, and tracking a certain trajectory whilst docked to the object being tracked, i.e. the wand.

The design of the gripper required for the research proved to work as intended. Although from a practical point of view, the proposed feedback control proved to be difficult due to the fact that full determination of the phalange location is impossible by means of the 3d tracking system and the absence of information about the physical object.

Unfortunately the idea of using a second UAV, i.e. the Ducted Fan, to perform some cooperative flying and grapsing proved difficult due to the instability of the platform. However the principle of cooperative grapsing has been illustrated by means of the experiments with the wand, provided a platform with a high attitude control is used.

Recommendations for future work

Althought the system is shown to work, some improvements and/or future extensions might be possible:

- Determine whether the proposed architecture works with a second UAV as well;
- Get the Ducted Fan to fly more stable, i.e. by equiping the ducted fan with onboard gyroscopes for a low level hard real-time attitude control loop;
- The gripper can be extended as well to support a VSA which enables handling of different object stiffnesses with a variable passive spring in stead of by means of control. Also support for pinching might be desirable;
- In order to apply all the proposed stratigies outside the external visual system should be removed and IMUs be used instead.

A Gripper design

The research presented in this report requires a gripper capable of interacting actively with the environment. The design, from concepts to a physical system, of such a gripper is detailed out below. At first several concepts are thought up or reviewed and modelled. Afterwards one design is chosen and physically created.

A.1 Requirements

The gripper should be mountable on the side of an aerial vehicle. This imposes several limitations. Due to the off centre location the total weight should be kept to a minimum. Also if possible the weight should be evenly distributed over the UAV in order to keep it statically balanced. With this in mind and taking goals of the project into account as well, a list of requirements can be formulated:

- The gripper should be underactuated due to weight constraints;
- Form closure should be achievable;
- Various object sizes, shapes and stiffnesses should be possible;
- Easily constructible.

A.2 Concepts

With the list of requirements in mind three concepts were thought up. All of these are modelled using 20-sim to figure out their feasibility and concordance to the requirements. In order to model the gripper concepts several parts had to be modelled from scratch. Among these an element to resemble physical contact between two objects was created and based on the Hunt-Crossley model with friction. Also several tendon structures were made as well as spring structure between two joints.

In the end all three concepts were modelled successfully which enabled comparison of them all and one could be chosen for physical creation.

Since form closure should be achievable a minimum of three fingers is required. Also all of the concepts are tendon driven to help with weight distribution. For convenience and clarity only one finger is drawn for each concept.

A.2.1 Concept One

A schematic of the first concept can be found in Figure 1. The principle behind the concept is that the rotational springs always tend to close the

finger, while the tendon pulling on the outmost phalange is used to keep the finger and thus the gripper open. The amount of force exerted on the tendon determines the configuration of the finger due to the equilibrium of forces

$$F_{tendon} + F_{springs} + F_{interaction} = 0 \tag{1}$$

so the system is force driven. Also the maximum amount of force that can be exerted on the environment is fully determined by the rotational springs.

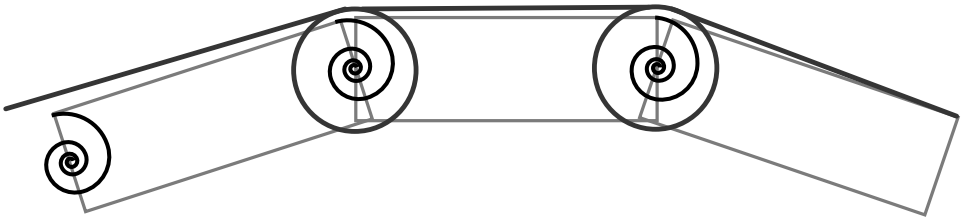

Figure 1: Schematic overview of one finger of the first gripper concept. The rotational springs ensore the finger closes, while pulling the tendon opens it.

An advantage of this system is that form closure is ensured.

Disadvantages of such a system is the fact that the force exerted on the environment is fully determined by the rotational spring force and the fact that the tendon is always loaded which in turn means that the motor will always have to deliver a force to the system.

A.2.2 Concept Two

The second concept relies on the ratio between in- and output pulleys of each phalange and the previous one and is loosely based on the work of M. Wassink. This means the system is position driven. In fact the trajectory of each of the phalanges is in fact fully determined due to these ratios. A schematic overview of the system can be found in Figure 2.

Advantages of this system are that it allows for controlled actuation back and forth and an unloaded tendon.

A disadvantage is that the motion profile is fully defined by the pulley ratios. Therefore form closure in terms of full contact with the environment cannot be guarenteed.

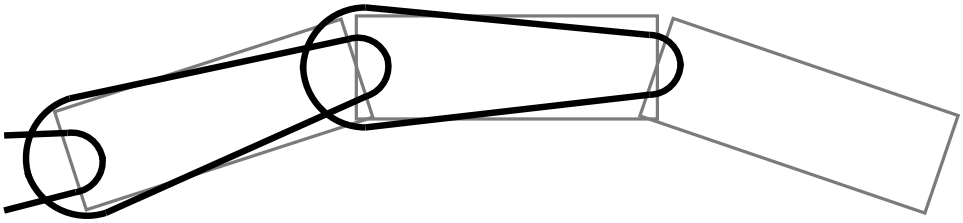

Figure 2: Schematic overview of one finger of the second gripper concept. The ratio between in- and output pulleys of each phalange fully determines the trajectory of the phalanges.

A.2.3 Concept Three

The third and final concept can be found in Figure 3 which is based on a proposal of Gert A. Kragten. This system is driven by tendons connected to the vertical phalange, imposing a rotation. All the other phalanges can rotate freely. The spring ensures the outmost phalange stays open untill the first bottom phalange hits the environment. When this occurs the outmost one rotates inward ensuring form closure.

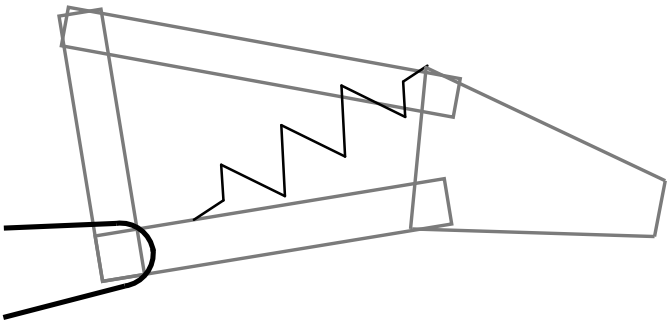

Figure 3: Schematic overview of one finger of the third gripper concept. The spring between the phalanges keeps the outmost phalange in its open state untill the first bottom phalanges is in contact with the environment.

Advantages of this concept are that it ensures form closure, is drivable in both directions and it requires a low operating force, slightly higher than the spring force is enough to close the gripper completely.

A disadvantage is the fact that the full trajectory of the phalanges is not fully determined by the freedom in rotation of most of the joints.

A.2.4 Comparison

In order to choose a concept, the concordance to the requirements for each is displayed in Table 1.

	Form closure	Variable objects	Constructibility
Concept One	+	+	0
Concept Two	-	0	+
Concept Three	+	+	+

Table 1: Comparison of concepts based on requirements

This table clearly shows that concept three has all the desired functionability. Therefore this design is chosen and converted to a physical prototype.

A.3 Physical realisation

This chapter describes the physical realisation of the chosen system. In order to do so both the gripper itself and a motor housing need to be designed as well as a connection in between. This to ensure a proper weight distribution of the subsystem over the UAV. The motor housing is connected to the gripper by means of bowden cables made of a steel inner cable coated with teflon, a teflon tube and a flexible steel outer shell.

A.3.1 Gripper

In order to realise the gripper itself physically the model needs to be adapted slightly. The main reason for this is that the current driving mechanism might hit objects in the gripper, which is unwanted. To overcome this problem the actuation is done via a rod connected to a pulley. The rod is in turn connected to the top joint of the vertical phalange. In essence this imposes the same rotation on the vertical phalange and thus results in the same workings. The result can be found in Figure 4

The dashed line in the figure shows how the tendon passes through the subsystem. The reason it crosses in the middle is to change the rotation of the top with respect to the bottom in order to ensure both top and bottom fingers close when bottom cable is pulled and open when the top cable is pulled in Figure 4. Effectively, this ensures a push-pull configuration allowing for both controlled opening and closing of the gripper.

A.3.2 Motor housing

The motor housing forms an interconnection between the motor and the tendons. To achieve this connection a pulley is used to which both the push and pull cable is connected. The technical drawing hereof can be seen in

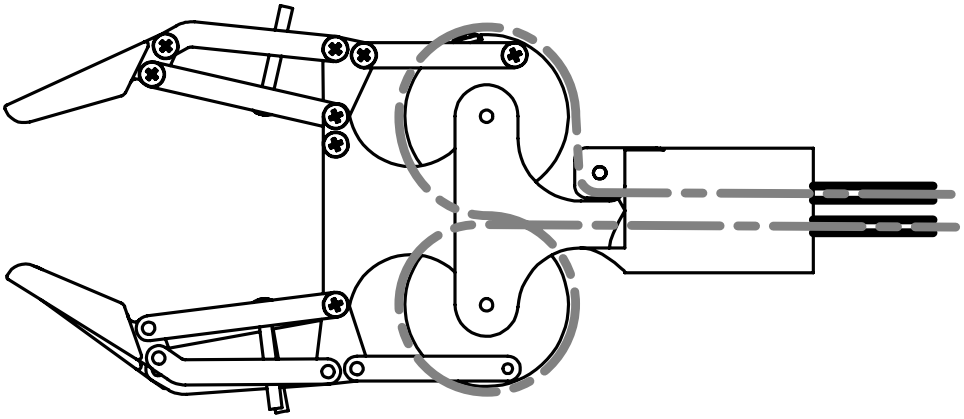

Figure 4: Technical drawing of the gripper along with the bowden cables drawn in (dashed line).

Figure 5 as well as the tendon connections. Note that bottom cable actually goes behind the pulley from this point of view.

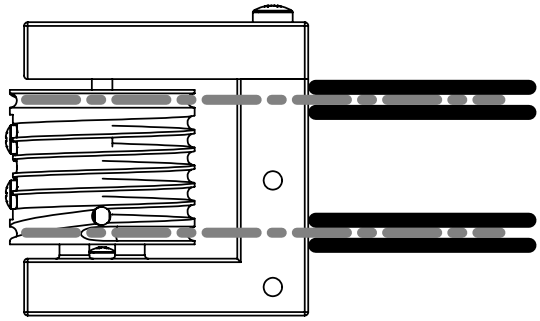

Figure 5: Technical drawing of the motor housing along with the bowden cables drawn in (dashed line).

B Ducted fan manual

The ducted fan is an unmanned aerial vehicle (UAV) designed by the University of Bologna. The aim of this article is to give a more in depth look into the inner workings of this UAV both from a hardware and software point of view. Also some insight is given into the mathematics behind the vehicle and some remarks about simulations will be made as well as some conclusions drawn.

B.1 Hardware

The hardware of the ducted fan can be divided into a mechanical and an electronical part.

B.1.1 Mechanics

From a mechanical point of view the ducted fan is composed of the following parts:

- A cylindrical duct that serves as the main body of the vehicle to which everything is connected;
- A main rotor that spans 280 millimeters, used for thrust generation;
- Eight vanes that are connected beneath the main rotor and can be used to direct the airflow.

The idea behind this mechanical setup is that by forcing air through the cylindrical duct by means of the main rotor lift is generated. In turn the vanes direct the flow of air in order to keep the vehicle upright as well as to steer it to a desired location.

B.1.2 Electronics

The electronics used in the system are the following:

- An Arduino ATMega2560 that is in charge of low level control;
- A Polulu Mini Maestro 12 board that is used to control all the actuators by means of its servo outputs;
- A Scorpion SII-3026-1190KV Brushless Motor that drives the main rotor;
- An Electronic Speed Controller (ESC) which controls the main rotor's speed based on the servo output it receives from the Polulu board;
- Eight Digital BB Carbon Gear Servos (HG-D202HB) to control the angle of the eight vanes;

- An xBee on an xBee Adapter for communication with the rest of the world;
- An Ultimate Battery Eliminator Circuit (UBEC) to generate a stable 5 V line;
- A 5S Lithium Polymer battery of 3400 mAh to supply power to the system;
- An AttoPilot, used to measure the current delivered by the battery pack to the system as well as the driving voltage.

The way all these different electronical components are connected to each other can be seen in Figure 6.

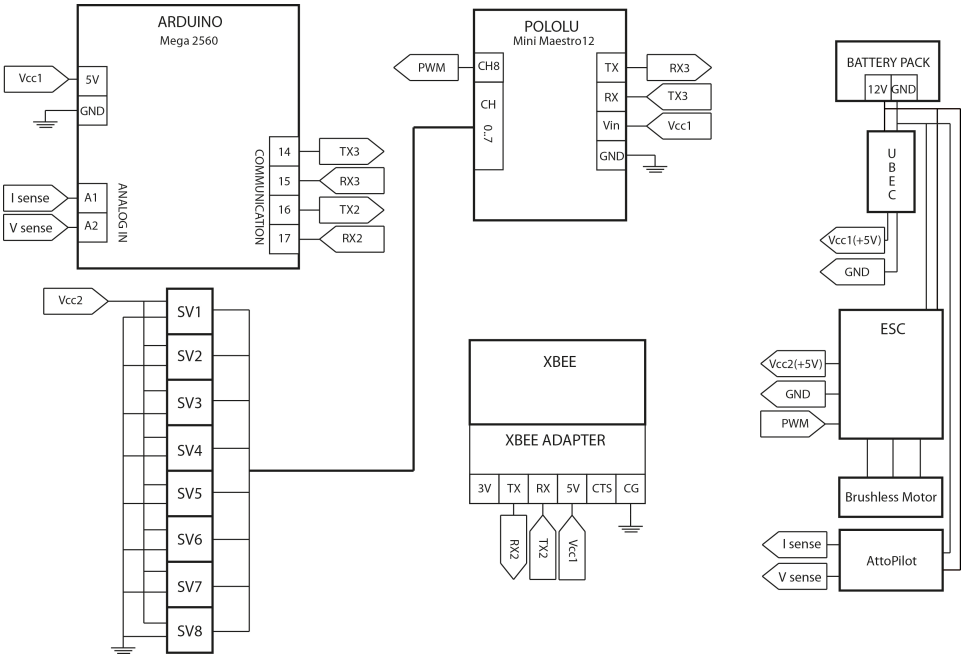

Figure 6: The interconnection of all the different electronical components

B.2 Software

In order to get the complete system to work, both low (embedded) and high level software is required. A schematic overview of the system flow can be found in Figure 7.

The low level software takes the form of C++ code for the Arduino that reads input messages relayed by the xBee over a TTL serial connection. The contents of these messages are setpoints for both the vanes and the main rotor. After some checking the parsed messages are relayed over another

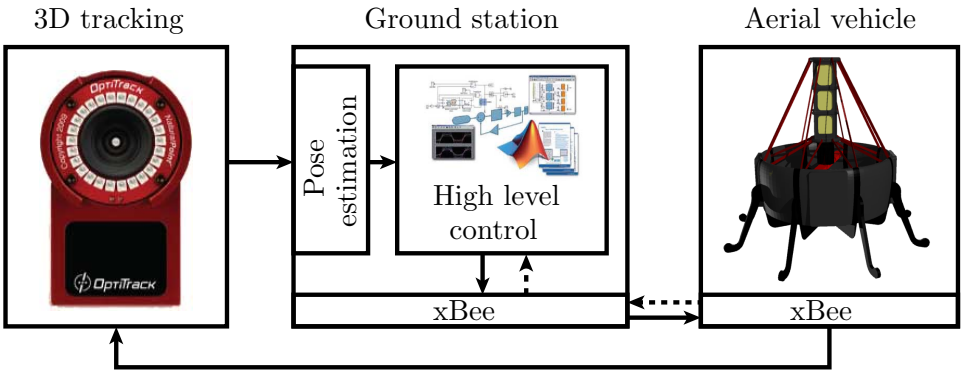

Figure 7: Schematic overview of the signal flow for the control of the ducted fan. Dashed lines indicate optional communication.

TTL serial connection to the Polulu board that in turn sets the appropriate servo outputs to the appropriate values. This all occurs at 50 Hz.

Optionally the Arduino can read out the sensed values from the AttoPilot and send these back to the high level control via the xBee. In practise the maximum available communication rate of the xBee (57600 kbps) deemed to low for this to happen simultaniously.

The high level software part of the system is constructed in Matlab Simulink and run via Windows Real-Time Target. This peace of software receives input from both an OptiTrack system, used to determine position and orientation of the UAV, as well as a PS3 controller, needed to steer the UAV. These inputs yield setpoints for the UAV which are converted to the appropriate format (servo values) and send as a stream to the xBee connected to the ground station.

B.3 Control & Simulation

In this section the dynamics and its control will be discussed briefly. Also some notes on simulation will be given.

B.3.1 Dynamics

The ducted fan is like the quadrocopter an underactuated system, since it has only four control inputs, i.e. the thrust T, and the angles α, β and γ of the vanes, and six degrees of freedom (DoF). Due to the mechanical design of the ducted fan, a net torque as well as force can be applied in any direction by varying the angles of the vanes. The mapping between the generated thrust of the rotor and the angles of the vanes and the total wrench exerted

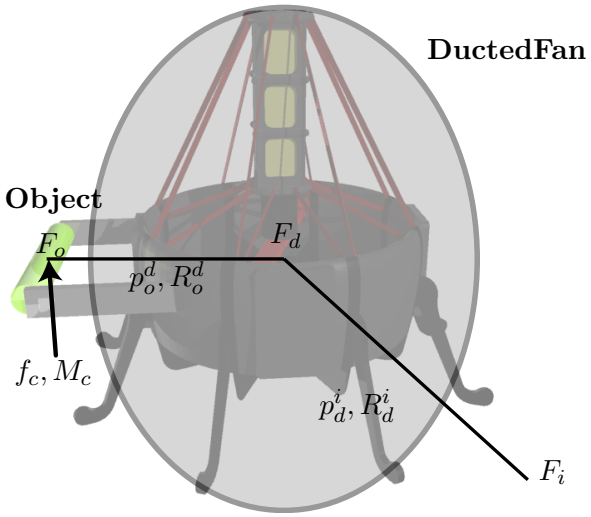

Figure 8: The ducted fan UAV and its reference frames.

on the UAV's c.g. is given by

$$\begin{bmatrix} M_x \\ M_y \\ M_z \\ f_x \\ f_y \\ f_z \end{bmatrix} = \begin{bmatrix} 0 & dTk_1 & 0 & 0 \\ 0 & 0 & dTk_1 & 0 \\ 0 & 0 & 0 & \frac{d_T}{2}Tk_2 \\ 0 & 0 & dTk_1 & 0 \\ 0 & dTk_1 & 0 & 0 \\ 1 & 0 & 0 & 0 \end{bmatrix} \begin{bmatrix} T \\ \alpha \\ \beta \\ \gamma \end{bmatrix} \tag{2}$$

where d is the distance between the UAV's c.g. and the centre of the vanes, and k_1 and k_2 the ratios between the propeller reaction torque and generated thrust. Using this and Figure 8 as a visual reference, the full dynamics of the UAV can be described by

$$\begin{aligned} m_{df}\dot{v}^i &= m_{df}g\hat{z}^i + R_d^i f_p^d + R_d^i R_o^d f_c^o \\ J_{df}\dot{\omega}_d^{d,i} &= -\omega_d^{d,i} \times J_{df}\omega_d^{d,i} + M_{gy}^d + M_p^d \\ &\quad + R_o^d M_c^o + R_o^d f_c^o \times p_o^d \end{aligned} \tag{3}$$

where $\dot{\omega}_d^{d,i}$ and $\omega_d^{d,i}$ are the rotational velocity and acceleration of the UAV with respect to the inertial frame, F_i, expressed in the ducted fan frame, F_d, respectively; $\dot{v}^i$ the linear acceleration of the UAV's c.g. in F_i; f_p^d the control force input and f_c^o the forces due to external input. R_a^b denotes a rotation of frame a with respect to frame b and p_a^b denotes a translation of frame a with respect to frame b.

B.3.2 Control

A similar approach as with the quadrotor can be applied to the ducted fan, i.e. assuming a high attitude control authority which reduces the ducted fan's system dynamics in Equation 3 to

$$m_{df}\dot{v}^i = m_{df}g\hat{z}^i + R^i_d f^d_p + R^i_d R^d_o f^o_c \tag{4}$$

where $R^i_d R^d_o f^o_c$ is the external force input due to the interaction with the other UAV via the bar shaped object. By letting

$$R^i_d f^d_p = u - m_{df}g\hat{z}^i \tag{5}$$

the system equation is reduced to something similar as the equations for the quadrotor UAV and the same further analysis applies.

B.3.3 Simulation

Using the above dynamics and control several simulations were done including cooperative flying with a quadrotor UAV. All of these seemed stable up to some level of disturbance. Also the path tracking capabilities were explored and seemd to be working sufficiently.

However when trying out the real hardware and control, the system turned out to be less stable than expected. The assumption of high attitude control, upon which the control architecture is based, turned out to be not valid. The cause of this might be due to the fact that the whole control architecture is run off-site, i.e. on a PC near the ducted fan and setpoints are relayed to it via xBee. This creates a lot of delay in the feedback and therefore causes instability.

In order to overcome these problems moving some of the control to the ducted fan itself by means of some gyroscopes or an IMU for instance, the high attitude controller can be run at a much higher frequency and have less delays as well.